Diffuse scattering from an $Al_{72}Ni_{20}Co_8$ decagonal quasicrystal on an order–disorder transformation

2003 J. Phys.: Condens. Matter 15 1665

(http://iopscience.iop.org/0953-8984/15/10/314)

INSTITUTE OF PHYSICS PUBLISHING JOURNAL OF PHYSICS: CONDENSED MATTER

J. Phys.: Condens. Matter **15** (2003) 1665–1676 PII: S0953-8984(03)53012-0

Diffuse scattering from an $Al_{72}Ni_{20}Co_8$ decagonal quasicrystal on an order–disorder transformation

H Abe[1], H Saitoh[2], T Ueno[2], H Nakao[3], Y Matsuo[4], K Ohshima[2] and H Matsumoto[1]

[1] Department of Materials Science and Engineering, National Defense Academy, 1-10-20 Hashirimizu, Yokosuka 239-8686, Japan
[2] Institute of Materials Science, University of Tsukuba, 1-1-1 Tennoudai, Tsukuba 305-8573, Japan
[3] Department of Physics, Tohoku University, Sendai 980-8578, Japan
[4] Department of Physics, Nara Women's University, Kitauoya-Higasi, Nara 630-8506, Japan

Received 4 September 2002
Published 3 March 2003
Online at stacks.iop.org/JPhysCM/15/1665

Abstract

Non-uniform distortion induced by superstructure domains has been observed during the ordering process of an order–disorder transformation in a single decagonal quasicrystal of $Al_{72}Ni_{20}Co_8$. The full width at half maximum (FWHM) of the fundamental reflections increased below the transformation temperature, T_c. At the same time, the integrated intensity of the fundamental reflections varied drastically at T_c. A small hysteresis was also observed in the temperature dependences of both the FWHM and the integrated intensity of the fundamental reflections. Peak broadening of the fundamental reflections is predominantly dependent on $|G^{\parallel}|$ below T_c. In addition, the weak dependence of the peak broadening with $|G^{\perp}|$ is extracted from the observed FWHM of the fundamental reflections. After deconvolution, the FWHM of the fundamental reflections appears to be a linear combination of $|G^{\parallel}|$ and $|G^{\perp}|$. Coexistence of the non-uniform distortion and of the random phason strain contributes to the ordering process below T_c. The diffuse scattering from atomic short-range order (SRO) was distributed around the ideal positions of the superstructure reflections. The SRO diffuse scattering disappeared completely above $T_c + 10$ K. In addition, a small hysteresis of the SRO diffuse scattering was found in the temperature cycle.

1. Introduction

The Al–Ni–Co (ANC) system is well known to be decagonal quasicrystals, which have two-dimensional (2D) quasiperiodic planes. The structures of ANC depend both on the Ni and Co concentrations and on temperature extensively. The complex phase diagram of ANC has

been reported in a previous study [1]. The phase diagram contains a great variety of phase transitions, i.e., quasicrystal-approximant phase transitions, phase transitions from 2D- to 1D-quasicrystal, order–disorder transformations, etc. Very recently, systematic interpretations of ANC structures were summarized in detail [2]. The various structures and columnar clusters of ANC were determined by electron diffraction analysis, high-resolution transmission electron microscopy (HRTEM) and high-angle annular dark-field scanning transmission electron microscopy (HAADF-STEM).

In this complex ANC system, the structure of $Al_{72}Ni_{20}Co_8$ was interpreted as an atomic decoration of ideal Penrose tiling [3, 4]. Moreover, it was reported that a decagonal columnar cluster of diameter 2 nm shows breaking of the tenfold symmetry [5, 6]. Recently, the structure of $Al_{72}Ni_{20}Co_8$ was determined by x-ray diffraction [7]. On the other hand, the analysis of the anomalous x-ray diffuse scattering showed the existence of atomic SRO [8]. The SRO diffuse scattering was only distributed in the quasiperiodic planes around the superstructure positions. These results were interpreted by 'chemical ordering', which is a pure atomic rearrangement on the average lattice sites. Furthermore, the SRO diffuse scattering consisted of the partial intensities from three kinds of atomic pairs, Al–Ni, Ni–Co and Co–Al. $Al_{72}Ni_{20}Co_8$ had no phason strain, since the distribution of each SRO diffuse scattering was isotropic. This is consistent with the fact that $Al_{72}Ni_{20}Co_8$ had no $|G^{\perp}|$ dependence of the FWHM of the fundamental reflections [8]. Here, $\boldsymbol{G}$ refers to the 5D reciprocal lattice vector, which consists of two components, $G^{\parallel}$ and $G^{\perp}$. $G^{\parallel}$ is the 3D reciprocal lattice vector in the physical space. $G^{\perp}$ is the 2D component in the complementary perpendicular space. A 'topological ordering' such as the phason strain is defined as the displacements from the average lattice points without atomic rearrangement. The concept of phasons (linear phasons and random phasons) was theoretically introduced in quasicrystals: a phason is an incommensurate atomic density wave representing a replacive defect [9]. In particular, a linear phason strain results in peak shifts from the ideal Bragg positions. The peak shifts increase with the values of $|G^{\perp}|$ [10]. On the other hand, a random phason strain causes peak broadening proportional to the $|G^{\perp}|$ values [11]. Very recently, local anomaly on the Debye–Waller factor was detected by *in situ* observations using HAADF–STEM [12]. This can be explained by the local dynamic fluctuations corresponding to phason flips excited at high temperature.

The structure of $Al_{70}Ni_{15}Co_{15}$ contains tenfold symmetric decagonal columnar clusters and a phason was observed in real space by HRTEM [13]. Furthermore, the anisotropic diffuse scattering derived from the phason strain was measured in anomalous x-ray scattering experiments [14]. For example, $|G^{\perp}|$ dependence of the FWHM of the fundamental reflections was observed in $Al_{70}Ni_{15}Co_{15}$. The SRO diffuse scattering depended on the incident x-ray energy. Further quantitative analysis showed that the SRO diffuse scattering of $Al_{70}Ni_{15}Co_{15}$ is explained by only one atomic pair, Ni–Co. This means that there is long-range order (LRO) between Al and the transition metals. It is predicted that an order–disorder transformation in $Al_{70}Ni_{15}Co_{15}$ possesses both 'chemical' and 'topological' orderings [14].

From the point of view of an order–disorder transformation, many studies have been recently carried out at high temperatures. For example, $Al_{70}Ni_{17}Co_{13}$ has two types of superstructures, S1 and type I (S1 + S2). The S2-superstructure of $Al_{70}Ni_{17}Co_{13}$ disappeared completely above T_c (=1123 K), while the S1-superstructure never vanished above T_c [15]. Here, the S1- and S2-superstructure reflections can be classified as $\sum_i h_i = \pm 1 \pmod 5$ and $\sum_i h_i = \pm 2 \pmod 5$. Temperature dependences of the diffuse scattering were reported in connection with the phase transformations in ANC [16, 17]. In particular, the S2-superstructure reflections of $Al_{72.7}Co_{11.6}Ni_{15.7}$ disappeared gradually between 990 and 1060 K, though the S1-superstructure reflections disappeared at approximately 1190 K. Very recently, Edagawa *et al* [18] showed evidence of the dynamic phason fluctuations by *in situ* HRTEM experiments

at high temperature. Slow atomic flipping between the equivalent positions was realized in an $Al_{65}Cu_{20}Co_{15}$ decagonal quasicrystal.

Considering the electronic structure of quasicrystals, the existence of SRO is important in explaining the absence of the theoretically predicted spikiness of the density of states (DOS). For example, a pseudogap, as predicted theoretically, on the electronic structure of $Al_{70}Ni_{15}Co_{15}$ has been reported [19], although the DOS spikiness was washed out. Full *ab initio* calculations were carried out using the modified short-range pair interactions to predict the structure of a decagonal quasicrystal of ANC [20].

Our goal is to understand the ordering process by measuring the SRO diffuse scattering and both $|G^{\parallel}|$ and $|G^{\perp}|$ dependences of the FWHM of the Bragg reflections during a high temperature cycle.

2. Experimental details

The diffuse scattering measurements were performed on beamline BL-4C of the Photon Factory at the High Energy Accelerator Research Organization in Japan. A cylindrical focusing mirror was placed in front of a double monochromator of Si(111). The sample was mounted on a four-circle diffractometer (Huber 5010). Air scattering was minimized by He filled beam paths. Fluorescence from the sample was reduced using a curved highly oriented pyrolytic graphite (002) (Panasonic Co.). The incident x-ray energy was calibrated to within 1 eV using Co foil. The incident x-ray energy was 7.686 keV near the Co K-edge so as to get a small absorption coefficient for $Al_{72}Ni_{20}Co_8$. The unit of the reciprocal space is $4\pi(\sin\theta)/\lambda$ (nm^{-1}). The resolution function of the reciprocal space for this beam optics was found to be 0.0123 (nm^{-1}) (0.0094°) using a Si single crystal. The high temperature vacuum furnace (Mac Science Co.) consists of two hemispherical Be windows of thickness 1 mm. The temperature in the furnace was stable to within 0.1 K. In order to analyse the diffuse scattering quantitatively (electron units/atom), we measured the several integrated intensities of a standard powder sample of Ni. The polarization factor $p = (1 + k_p \cos^2 2\theta)/(1 + k_p)$ was experimentally determined to be defined by $k_p = 0.0279$ by fitting the intensities of the Bragg reflections of the Ni powdered sample. The calculated Compton scattering was subtracted from the normalized diffuse scattering.

An alloy ingot with nominal composition $Al_{72}Ni_{20}Co_8$ was prepared by melting mixtures of pure Al (99.99%), Ni (99.99%) and Co (99.99%) metals under an Ar atmosphere in an arc furnace. This ingot was crushed into powder, put into an alumina crucible and then sealed in a quartz tube. The powder sample was melted at 1423 K, slowly cooled to 1073 K at the rate of 50 K h^{-1}, kept at 1073 K for 1 day and then quenched in water ($T_q = 1073$ K). The sample was approximately rod shaped (length 0.64 mm, diameter 0.08 mm). The mosaicity of the sample using the $1\bar{2}\bar{5}\bar{4}0$ fundamental reflection was estimated to be 0.0223 nm^{-1}(0.0198°). Here, the indexing of the Bragg reflections is the same as that used in a previous study [15]. For absorption corrections, we collected the equivalent Bragg reflections and calculated the absorption factors semi-empirically by a numerical scheme. In order to observe the ordering process in an order–disorder transformation, the following thermal treatments were carried out. The sample was heated rapidly from room temperature to 1116 K within 10 min. After that, the temperature cycle consisted of the following two steps: the first step was the cooling process from 1116 K down to 965 K and the second step was the heating process from 965 K up to 1096 K.

3. Results and discussion

Figure 1(a) shows temperature dependence of the FWHM for the radial scan of the $1\bar{2}\bar{5}\bar{4}0$ fundamental reflection. Here, the observed FWHM were deconvoluted using the resolution function, which was estimated by the Bragg reflections in a single Si crystal. There is a clear sharp bend in the line at T_c (=992 K). The abrupt increase of the FWHM of the fundamental reflection below T_c reveals the non-uniform distortion generated by the S1-type micro domain. The FWHM of the Bragg reflections are generally proportional to the $|G^{\parallel}|$ values under a non-uniform strain for conventional crystals, whereas a uniform strain provides peak shifts. In an AlCuLi approximant, peak broadening was predominantly caused by the non-uniform strain due to the microstructure-generated internal stresses [21]. The intrinsic defects annealed out at high temperature. In quasicrystals, the formation of microdomains was proposed theoretically in [22] to explain quasicrystal transformations, where each microdomain has no smooth boundary. The integrated intensities of the $1\bar{2}\bar{5}\bar{4}0$ fundamental reflection also changed drastically at T_c as shown in figure 1(b). Note that a hysteresis both of the FWHM and the integrated intensity of the fundamental reflection was estimated to be 10 K at approximately 992 K considering experimental error. This indicated that the order–disorder transformation of $Al_{72}Ni_{20}Co_8$ is a nearly second-order phase transition.

In order to separate the contributions of the non-uniform deformation and of the random phason strain, we measured the FWHM of the various fundamental reflections at 300 K (quenched above T_c), 965 K ($<T_c$) and 1096 K ($>T_c$). In many cases, peak broadening as a function of $|G^{\parallel}|$ and $|G^{\perp}|$ correspond respectively to the non-uniform deformation and the random phason strain. Here, the FWHM of the fundamental reflections were obtained by the radial scan on the 0th plane ($Q_z = 0$) only. The observed FWHM were also deconvoluted using the resolution function as mentioned earlier. Small peak broadening as a function of $|G^{\parallel}|$ of the fundamental reflections was found at room temperature in the as-quenched sample ($T_q > T_c$) as shown in figure 2. This means that only small deformation was induced by the quenching process. No increase of the FWHM of the fundamental reflections was seen at 1096 K ($>T_c$). In contrast, large $|G^{\parallel}|$ dependence of the fundamental reflections at 965 K ($<T_c$) was observed. This can be interpreted by the non-uniform deformations introduced by the S1 microdomains below T_c as mentioned earlier. If we look into details, it should however be noted that some data points do not coincide exactly with the linear increase in the $|G^{\parallel}|$ axis. We believe that these disagreements with the $|G^{\parallel}|$-linearity imply the existence of the random phason strain in the $|G^{\perp}|$ axis below T_c. The non-uniform deformation and the random phason strain occur simultaneously on an order–disorder transformation. Thereby the observed FWHM, $\eta^{obs}(|G^{\parallel}|, |G^{\perp}|)$, were separated into the $|G^{\parallel}|$ and $|G^{\perp}|$ components. The observed FWHM of the fundamental reflections have a simple relationship in the $|G^{\parallel}|$ and $|G^{\perp}|$ components given by,

$$\eta^{obs}(|G^{\parallel}|, |G^{\perp}|) = \eta^{\parallel} + \eta^{\perp} = \alpha|G^{\parallel}| + \beta|G^{\perp}|. \tag{1}$$

Figure 3(a) is the $|G^{\parallel}|$ plot of $\eta^{obs}(|G^{\parallel}|, |G^{\perp}|)$, where the observed FWHM of the fundamental reflections are projected onto the $|G^{\parallel}|$ axis. The solid line in figure 3(a) shows the lower limit of the observed FWHM as a function of $|G^{\parallel}|$, that is, $\alpha|G^{\parallel}|$. After deconvolution of the $|G^{\parallel}|$ component, the deconvoluted FWHM, $\eta^{\perp}(|G^{\perp}|)$, are plotted as a function of $|G^{\perp}|$ in figure 3(b). A linear fit of the deconvoluted data is displayed in the solid line in figure 3(b). The fitted slope of $\eta^{\perp}(|G^{\perp}|)$ is equal to β ($=\mathrm{d}\eta^{\perp}/\mathrm{d}|G^{\perp}|$). Using this β value, we apply to the deconvoluted FWHM along $|G^{\parallel}|$, that is, $\eta^{\parallel}(|G^{\parallel}|)$. The results show good agreement with the $|G^{\parallel}|$-linearity in figure 3(c). The relation expressed in equation (1) is appropriate, since two kinds of the deconvoluted FWHM are self-consistent with each other within experimental

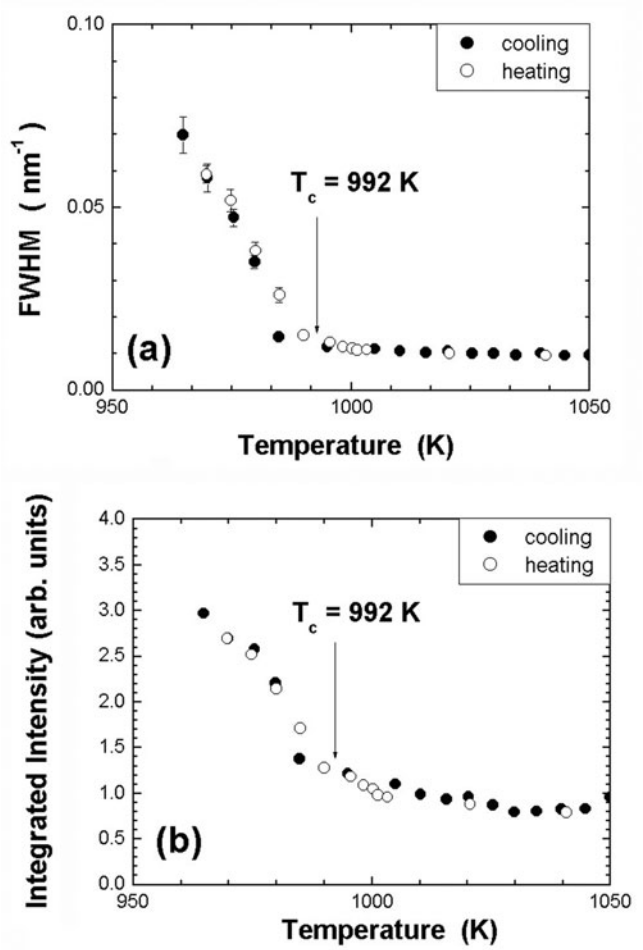

Figure 1. Temperature dependences of (a) the FWHM and (b) the integrated intensity for the radial scan of the $1\bar{2}\bar{5}\bar{4}0$ fundamental reflection.

error. The actual α and β values are 0.001 60 and 0.000 565, respectively. The β values both at room temperature (the as-quenched sample) and at 1096 K ($>T_c$) are almost negligible. The slope of the FWHM along $|G^{\perp}|$, β is a measure of the magnitude of the random phason strain. Therefore, a random phason contributes to an order–disorder transformation, since β below T_c is larger than at 1096 K ($>T_c$) by *in situ* observations. Compared with other ANC systems, the β values are shown in table 1. Obviously, the β value of $Al_{72}Ni_{20}Co_8$ at 965 K ($<T_c$) is much smaller than other ANC systems (the as-quenched samples). Moreover, the different densities among ANC systems reflect the presence of different kinds of defect at room temperature. For example, the ratio of atomic weight between $Al_{70}Ni_{15}Co_{15}$ and $Al_{72}Ni_{20}Co_8$ is 1.02 and the ratio of density between them is 1.14. It is clear that the Co concentrations can control the phason strain on the transformations in ANC.

Figures 4(a)–(c) show the distributions of the diffuse scattering around the $1\bar{2}\bar{5}\bar{4}0$ fundamental reflection at 300 K (quenched from above T_c), 965 K ($T < T_c$) and 1116 K ($T > T_c$), respectively. Here, the intensity is in electron units. Each interval in the contour

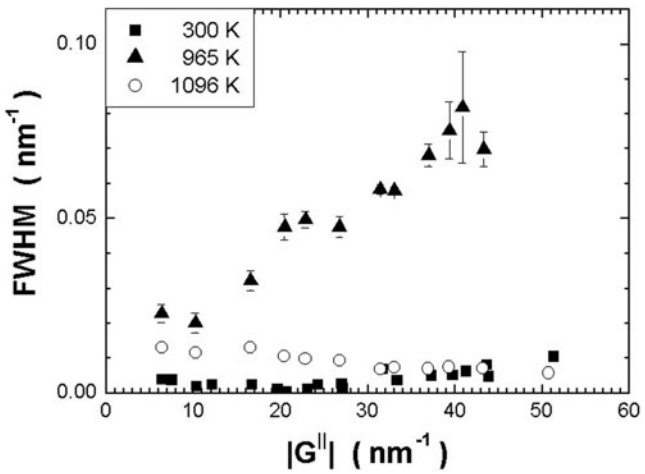

Figure 2. $|G^{\|}|$ dependences of the FWHM of the fundamental reflections at 300 K (quenched above T_c), 965 K ($T < T_c$) and 1096 K ($T > T_c$). Apparent peak broadening with increasing the $|G^{\|}|$ values at 965 K is observed.

Table 1. Fundamental data in the ANC system. a_0 is the lattice constant and $2a_0/\sqrt{5}$ is the edge length of the Penrose pattern. c_0 is the lattice constant along the periodic direction.

	$Al_{72}Ni_{20}Co_8$	$Al_{70}Ni_{15}Co_{15}$	$Al_{72.7}Ni_{8.5}Co_{18.8}$	$Al_{70}Ni_{10}Co_{20}$
Diffuse scattering	Isotropic	Anisotropic	Anisotropic and peak shifts	?
$d\eta/d\|G^{\perp}\|$	0.000 56 (965 K)	0.003 45	0.004 24	0.0098
a_0 (nm)	0.272 3	0.274 4	0.275 3	0.2768
c_0 (nm)	0.408 1	0.407 8	0.408 0	?
Density (g cm^{-3})	3.94	4.5	?	?

maps is 2.0 electron units. Each distribution was almost the same as the one in our previous study [8]. For example, the isotropic distributions of the SRO diffuse scattering appeared around the ideal positions of the fundamental reflection and the S1-superstructure reflections. In particular, only broad peaks without sharp peaks were located around the centre of the S1-superstructure positions (see white crosses in figure 4(a)). The distribution of the diffuse scattering around the fundamental reflection was isotropic as shown in figure 4(a). In general, the static strains cause asymmetric modulation of the diffuse scattering. It is considered that no phason strain contributes to the diffuse scattering. The absence of the phason strain is also supported by no $|G^{\perp}|$ dependence of the FWHM of the fundamental reflections at room temperature. The SRO diffuse scattering around the S1-superstructure positions at high temperature has a significant relationship with an order–disorder transformation. In figure 4(c), the SRO diffuse scattering around the S1 positions disappeared completely at 1116 K ($T > T_c$), though the SRO diffuse scattering was observed around the same positions below T_c (figure 4(b)). On the other hand, it is still unclear why much broader SRO diffuse peaks from the as-quenched sample was observed at room temperature. One of the possible reasons is that the quenching temperature, T_q (=1073 K), is much higher than T_c (= 992 K). For a comparison, the FWHM of the diffuse peak in the centre of line P ($2\bar{1}5\bar{2}0$ superstructure reflection) was found to be 0.713 (nm^{-1}) at room temperature. The diffuse peak width at

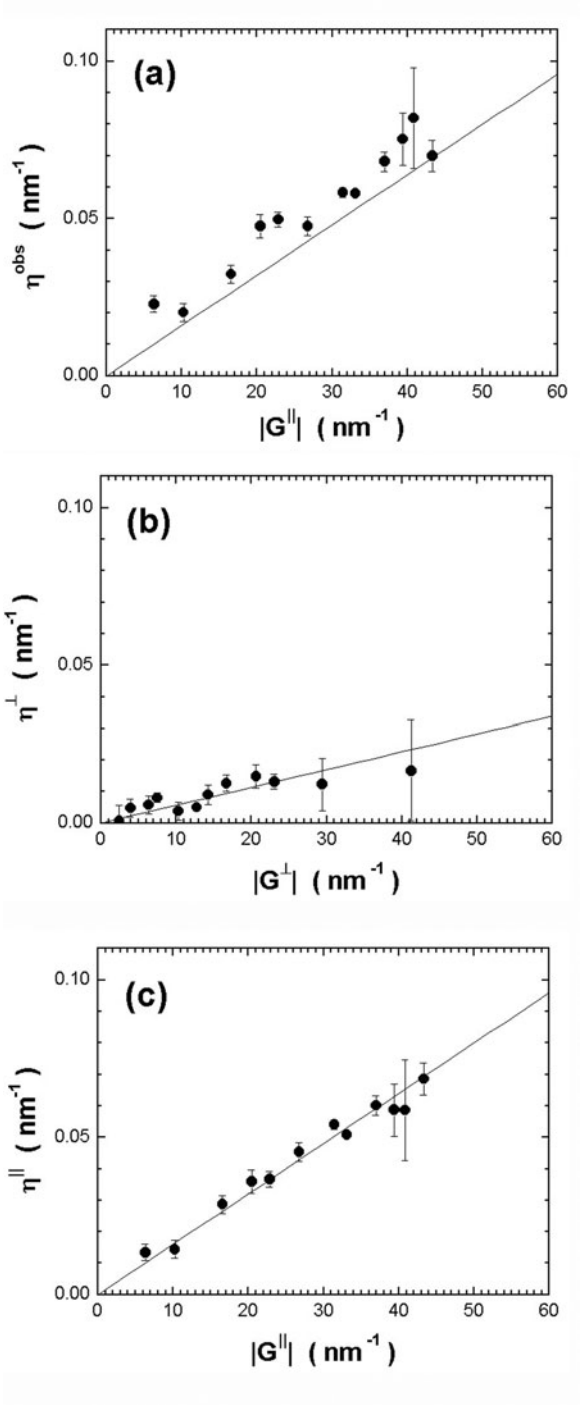

Figure 3. (a) Peak broadening as a function of $|G^{\parallel}|$ at 965 K ($T < T_c$). The solid line in figure 3(a) shows the lower limit of the observed FWHM of the fundamental reflections. (b) The deconvoluted FWHM as a function of $|G^{\perp}|$. The solid line is a linear fit on $|G^{\perp}|$ using the deconvoluted data. (c) The deconvoluted FWHM as a function of $|G^{\parallel}|$. The solid line, which is the same one as in figure 3(a), is the lower limit of the observed FWHM of the fundamental reflections.

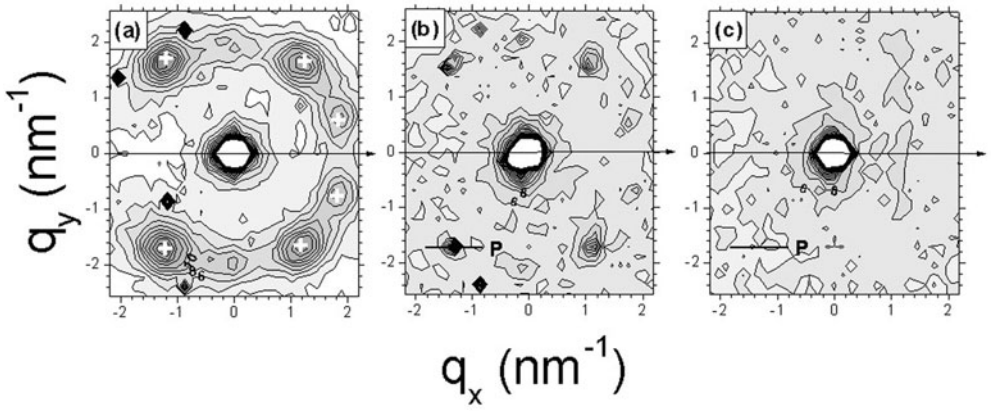

Figure 4. The reciprocal maps showing the SRO diffuse scattering around the $1\bar{2}\bar{5}\bar{4}0$ fundamental reflection at (a) room temperature (quenched above T_c), (b) 965 K ($T < T_c$) and (c) 1116 K ($T > T_c$). The white crosses are the ideal S1-superstructure positions. The diffuse intensity profile of the diffuse peak labelled P was measured during the temperature cycle in figure 5. The diffuse scattering around the S1-superstructure positions disappeared completely above $T_c + 10$ K.

the same position was approximately 0.20 (nm^{-1}) around T_c. From measurements along the periodic direction, Q_z, we found that the diffuse scattering is distributed on the quasiperiodic planes but not along the periodic direction. Considering the as-quenched sample ($T_q > T_c$), this means that 1D SRO (chain-like correlation) occurs mainly along the periodic direction as the precursor phenomenon of the formation of the S1 microdomains. In addition, the chain-like correlation accompanies the weak correlations with other neighbour chains parallel to the periodic directions, since the observed diffuse sheets are modulated on the S1-superstructure positions. The fit of the observed diffuse scattering profile was obtained by a Lorentzian function using the assumption of the Ornstein–Zernike correlation function [23]. This function is given by,

$$\chi(r) = \frac{1}{r}\mathrm{e}^{-r/\xi}, \tag{2}$$

$$\chi(k) = \frac{4\pi}{k^2 + 1/\xi^2}, \tag{3}$$

where ξ is the correlation length, which was estimated to be 2.8 nm at room temperature. On the other hand, the correlation length of the S1-type diffuse peaks increased to 11.0 nm at 965 K. The SRO analysis of the diffuse scattering enables us to determine both the atomic arrangements and the correlation length.

More detailed temperature dependence of the diffuse intensity at the peak maximum is shown in figure 5(a). The SRO diffuse intensity around the S1-superstructure reflection $(2\bar{1}\bar{5}\bar{2}0)$ was obtained by making a line scan (line P) as drawn in figures 4(b) and (c). The SRO diffuse intensity in ternary alloy systems is described by [24],

$$I^{SRO}(\boldsymbol{Q}) \propto x_A x_B |f_A - f_B|^2 \alpha^{A,B}(\boldsymbol{Q}) + x_B x_C |f_B - f_C|^2 \alpha^{B,C}(\boldsymbol{Q}) + x_C x_A |f_C - f_A|^2 \alpha^{C,A}(\boldsymbol{Q}), \tag{4}$$

$$\alpha^{A,B}(\boldsymbol{Q}) = \sum_l \alpha_l^{AB} \exp(-\mathrm{i}\boldsymbol{Q}\cdot\boldsymbol{R}_l), \tag{5}$$

where $\alpha^{m,n}(\boldsymbol{Q})$ are Fourier transforms of the Warren–Cowley SRO parameters. x_A, x_B and x_C are the concentrations of each kind of atom. R_l is the atomic position for the lth site in

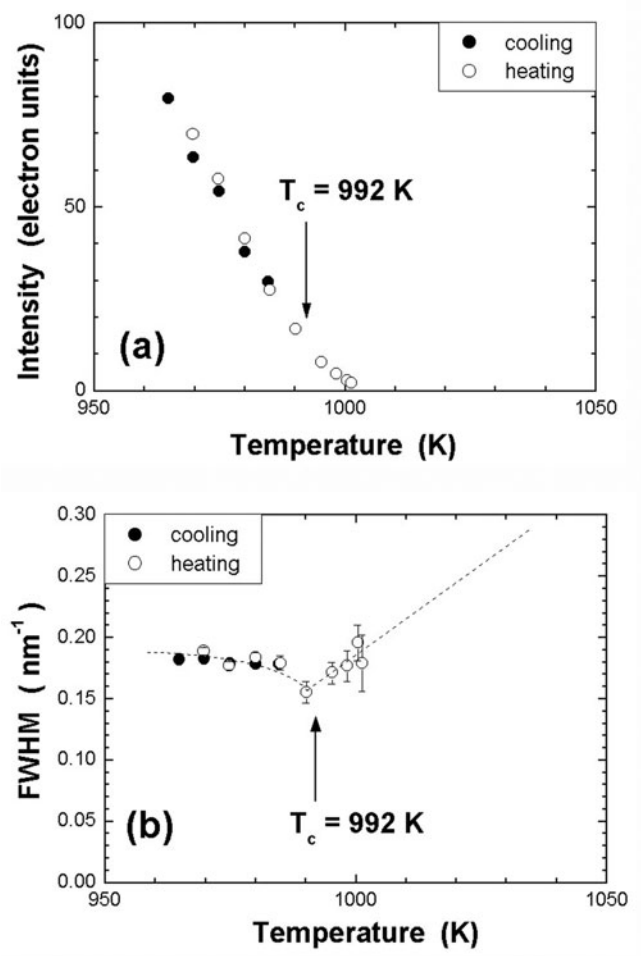

Figure 5. Temperature dependences of (a) the diffuse intensity and (b) the FWHM of the diffuse peak along line P in figure 4. The dotted curve is a guide for the reader's eye. A little hysteresis was shown in the temperature cycle.

the real space. The diffuse shape depends mainly on two properties described in equation (5). The value of α_l^{mn} stands for the ordering states in real space. This corresponds to the diffuse intensities in reciprocal space. The decay of α_l^{mn} with increasing R_l depends on the correlation length. Hence, the FWHM of the SRO diffuse scattering are determined by the α_l^{mn} decay. Two features of the SRO diffuse intensity as a function of temperature must be pointed out in the experimental results. One is that the diffuse intensities showed a small hysteresis in the temperature cycle. The other is the gradual increase of the SRO diffuse intensities indicating the ordering process.

The former reveals that the order–disorder transformation in $Al_{72}Ni_{20}Co_8$ is a near second-order phase transition. The latter indicates that the atomic rearrangements described by α_l^{mn} were taking place due to the continuous increase of the SRO diffuse intensity. The small SRO diffuse intensity around the S1-superstructure position did not vanish even above T_c but disappeared completely above T_c + 10 K. The FWHM of the SRO diffuse scattering had a minimum value around T_c (figure 5(b)), though the monotonic increase of the diffuse intensity

was seen on cooling as shown in figure 5(a). In general, the diffuse peak width is inversely proportional to the correlation length connected with the ordering process. On cooling, the correlation length continuously increases toward T_c indicating ordering. However, the diffuse peaks do not sharpen monotonically on cooling in $Al_{72}Ni_{20}Co_8$, since the SRO diffuse peaks are also modified by the non-uniform strains such as peak broadening of the fundamental reflections below T_c. The competition between peak sharpening and peak broadening leads to the minimum value of the FWHM around T_c. Actually, peak broadening of the fundamental reflections occurred below T_c in figure 1(a). In order to discuss the possibility of the peak sharpening and broadening, we estimate peak broadening on the S1-superstructure $(2\bar{1}\bar{5}\bar{2}0)$ position. At fixed temperature, peak broadening both on $|G^{\parallel}|$ and $|G^{\perp}|$ are proportional to the $|G^{\parallel}|$ and $|G^{\perp}|$ values in equation (1). The FWHM in the S1 $(2\bar{1}\bar{5}\bar{2}0)$ position becomes $\alpha|G^{\parallel}(2\bar{1}\bar{5}\bar{2}0)| + \beta|G^{\perp}(2\bar{1}\bar{5}\bar{2}0)|$ at 965 K. Here, we assume that the ratio of $\alpha(T)/\beta(T)$ is constant ($\alpha = 2.83\beta$) below T_c. Thus, temperature dependence of the FWHM is given by $\eta(T, |G^{\parallel}|, |G^{\perp}|) = \beta(T) \times (2.83|G^{\parallel}| + |G^{\perp}|)$. By substituting the $|G^{\parallel}|$ and $|G^{\perp}|$ values into the above equation, temperature dependence of the peak width of the $1\bar{2}\bar{5}\bar{4}0$ fundamental reflection, $\eta(T, 1\bar{2}\bar{5}\bar{4}0)$, becomes $126.1\beta(T)$. $\eta(T, 2\bar{1}\bar{5}\bar{2}0)$ is $140.9\beta(T)$. To estimate $\eta(T, 1\bar{2}\bar{5}\bar{4}0)$, we introduce the reduced temperature, $t(=T/T_c - 1)$. $\eta(-t, 1\bar{2}\bar{5}\bar{4}0)$ below T_c is fitted as $\eta(-t) = |-t|^{\gamma}$ as shown in figure 6(a), where γ is a parameter determined by fitting using the $1\bar{2}\bar{5}\bar{4}0$ fundamental reflection. From the relationship written by $|-t|^{\gamma} = 126.1\beta(T)$, temperature dependence of the FWHM of $2\bar{1}\bar{5}\bar{2}0$ becomes $\frac{140.9}{126.1} \times |-t|^{\gamma}$ by the assumption of the constant ratio of $\alpha(T)/\beta(T)$. Therefore, the deconvoluted FWHM at the $2\bar{1}\bar{5}\bar{2}0$ superstructure position is displayed in figure 6(b). Temperature dependence of the FWHM at this position shows a decrease on cooling. The correlation length develops gradually with decreasing temperature. We summarize our interpretation of the minimum value of the FWHM around T_c as follows. At the early stage of ordering above T_c, the small SRO regions become larger without distortion. Around T_c, the small 1D S1 microdomains, which are slightly distorted regions, are formed parallel to the periodic direction. Simultaneously, the SRO diffuse scattering starts to change to the superstructure reflection (peak sharpening). Consequently, the whole quasicrystal is distorted inhomogeneously due to the randomly located S1 domain parallel to the periodic direction and its size distribution (peak broadening).

4. Conclusions

An order–disorder transformation in $Al_{72}Ni_{20}Co_8$ was found to be a near second-order phase transition by temperature dependences of the diffuse intensity, the diffuse peak width, the integrated intensity and the FWHM of the fundamental reflection. A 10 K hysteresis at high temperature (992 K) is regarded as a small hysteresis thermodynamically, although a hysteresis means a first-order phase transition.

The pure development of SRO is realized only above T_c. It seems that there is no random phason strain at this temperature region because no $|G^{\perp}|$ dependence of the fundamental reflections was observed. The modulations on the S1-superstructure positions of the diffuse sheets show that there are the chain-like correlations along the periodic direction accompanying the weak inter-chain correlations above T_c. These chain-like correlations above T_c have a relation with nucleation of the rod shaped S1 microdomains below T_c. Further, the SRO diffuse intensity increased and the FWHM of the diffuse peak decreased on cooling. Below T_c, the S1 microdomains appeared parallel to the periodic direction and grew independently. This results in peak broadening of the fundamental reflections both on $|G^{\parallel}|$ and $|G^{\perp}|$, where the $|G^{\parallel}|$ component corresponds to the non-uniform deformation and the $|G^{\perp}|$ one to the random

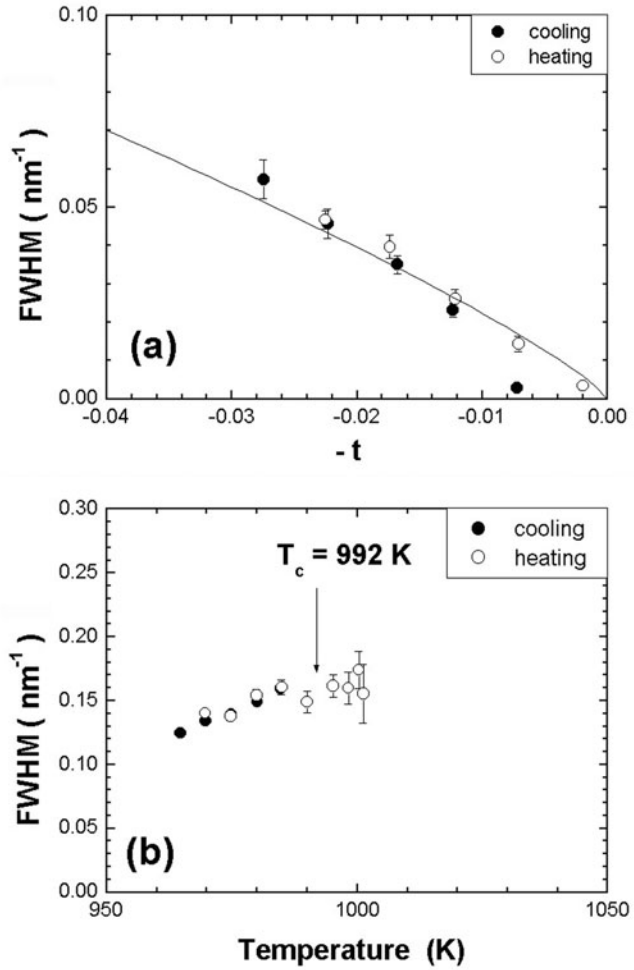

Figure 6. (a) Temperature dependence of the FWHM of the $1\bar{2}\bar{5}\bar{4}0$ fundamental reflection. The solid curve represents a fit to the $|-t|^{\gamma}$ function (see text). (b) The deconvoluted FWHM in the S1-superstructure reflection ($2\bar{1}\bar{5}\bar{2}0$) decreases with decreasing temperature.

phason strain. Even in the S1-superstructure reflections, the effect of peak broadening induced by distortion is not ignored. Actually, we can explain some experimental results using this idea. The minimum value of peak width on the S1-superstructure position around T_c originates from peak sharpening and broadening. Peak sharpening is the process from SRO to LRO on cooling, while peak broadening is caused by two kinds of distortion below T_c. We conclude that a random phason is the intrinsic property of an order–disorder phase transition even in $Al_{72}Ni_{20}Co_8$ regarded as the prototype of Penrose tiling. A random phason has connection with the formation of the S1 microdomain, since the S1-superstructure requires the local atomic flip.

Acknowledgments

The authors are grateful to professor Y Ishii of Chuo University, Dr A Yamamoto, Dr E Abe and Dr H Takakura of the National Institute for Materials Science for helpful discussions.

References

[1] Ritsch S, Beeli C, Nissen H-U, Godecke T, Scheffer M and Luck R 1998 *Phil. Mag. Lett.* **78** 67
[2] Hiraga K, Ohsuna T, Sun W and Sugiyama K 2001 *Mater. Trans. JIM* **42** 2354
[3] Ritsch S, Beeli C, Nissen H-U, Godecke T, Scheffer M and Luck R 1996 *Phil. Mag. Lett.* **74** 99
[4] Tsai A P, Fujiwara A, Inoue A and Msumoto T 1996 *Phil. Mag. Lett.* **74** 233
[5] Saitoh K, Tsuda K, Tanaka M, Kaneko K and Tsai A P 1997 *Japan. J. Appl. Phys.* **36** L1404
[6] Abe E, Saitoh K, Takakura H, Tsai A P, Steinhardt P J and Jeong H-C 2000 *Phys. Rev. Lett.* **84** 4609
[7] Takakura H, Yamamoto A and Tsai A P 2001 *Acta Crystallogr.* A **57** 576
[8] Abe H, Matsuo Y, Saitoh H, Kusawake T, Ohshima K and Nakao H 2000 *Japan. J. Appl. Phys.* **39** L1111
[9] Lubensky T C, Socolar J E S, Steinhardt P J, Bancel P A and Heiney P A 1986 *Phys. Rev. Lett.* **57** 1440
[10] Yamamoto K, Yang W, Nishimura Y and Matsuo Y 2002 *J. Alloys Compounds* **342** 237
[11] Matsuo Y, Sugiyama N and Yamamoto K 1999 *Mater. Trans. JIM* **40** 137
[12] Abe E, Pennycook S J and Tsai A P 2003 *Nature* **421** 347
[13] Hiraga K, Lincoln F J and Sun W 1991 *Mater. Trans. JIM* **32** 308
[14] Abe H, Tamura N, Le Bollo'h D, Moss S C, Matsuo Y, Ishii Y and Bai J 2000 *Mater. Sci. Eng.* **294–296** 299
[15] Edagawa K, Sawa H and Takeuchi S 1994 *Phil. Mag. Lett.* **69** 227
[16] Hradil K, Proffen T, Frey F, Kek S, Krane H G and Wroblewski T 1995 *Phil. Mag.* B **71** 955
[17] Baumgarte A, Schreuer J, Estermann M A and Steurer W 1997 *Phil. Mag.* A **75** 1665
[18] Edagawa K, Suzuki K and Terauchi S 2000 *Phys. Rev. Lett.* **85** 1674
[19] Stadnik Z M, Purdie D, Garnier M, Baer Y, Tsai A P, Inoue A, Edagawa K, Takeuchi S and Buschow K H J 1997 *Phys. Rev.* B **55** 10938
[20] Mihalkovic M, Al-Lehyani I, Cockayne E, Henley C L, Moghadam N, Moriarty J A, Wang Y and Widom M 2002 *Phys. Rev.* B **65** 104205
[21] Poon S J, Dmowski W, Egami T, Shen Y and Shiflet G J 1987 *Phil. Mag. Lett.* **56** 259
[22] Honal M, Haibach T and Steurer W 1998 *Acta Crystallogr.* A **54** 374
[23] Stanley H E 1971 *Introduction to Phase Transitions and Critical Phenomena* (Oxford: Clarendon)
[24] Hashimoto S 2000 *Acta Crystallogr.* A **56** 85